Bone 172 (2023) 116779

Contents lists available at ScienceDirect

Bone

journal homepage: www.elsevier.com/locate/bone

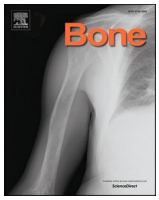

Full Length Article

Loss of hyaluronan synthases impacts bone morphology, quality, and mechanical properties

Meghana Pendyala [a,b], Samuel J. Stephen [a,b], Deepak Vashishth [a,b], Elizabeth A. Blaber [a,b,c,1], Deva D. Chan [a,d,*,1]

[a] Department of Biomedical Engineering, Rensselaer Polytechnic Institute, 110 8th St. Troy, NY 12180, United States of America
[b] Center for Biotechnology and Interdisciplinary Studies, Rensselaer Polytechnic Institute, 110 8th St. Troy, NY 12180, United States of America
[c] Blue Marble Space Institute of Science at NASA Ames Research Center, PO Box 1, Moffett Field, CA 94035, United States of America
[d] Weldon School of Biomedical Engineering, 206 S. Martin Jischke Drive, Purdue University, West Lafayette, IN 47907, United States of America

ARTICLE INFO

Keywords:
Hyaluronan
Hyaluronan synthase
Bone quality

ABSTRACT

Hyaluronan, a glycosaminoglycan synthesized by three isoenzymes (Has1, Has2, Has3), is known to play a role in regulating bone turnover, remodeling, and mineralization, which in turn can affect bone quality and strength. The goal of this study is to characterize how the loss of *Has1* or *Has3* affects the morphology, matrix properties, and overall strength of murine bone. Femora were isolated from *Has1*$^{-/-}$, *Has3*$^{-/-}$, and wildtype (WT) C57Bl/6 J female mice and were analyzed using microcomputed-tomography, confocal Raman spectroscopy, three-point bending, and nanoindentation. Of the three genotypes tested, *Has1*$^{-/-}$ bones demonstrated significantly lower cross-sectional area ($p = 0.0002$), reduced hardness ($p = 0.033$), and lower mineral-to-matrix ratio ($p < 0.0001$). *Has3*$^{-/-}$ bones had significantly higher stiffness ($p < 0.0001$) and higher mineral-to-matrix ratio ($p < 0.0001$) but lower strength ($p = 0.0014$) and bone mineral density ($p < 0.0001$) than WT. Interestingly, loss of *Has3* was also associated with significantly lower accumulation of advanced glycation end-products than WT ($p = 0.0478$). Taken together, these results demonstrate, for the first time, the impact of the loss of hyaluronan synthase isoforms on cortical bone structure, content, and biomechanics. Loss of *Has1* impacted morphology, mineralization, and micron-level hardness, while loss of *Has3* reduced bone mineral density and affected organic matrix composition, impacting whole bone mechanics. This is the first study to characterize the effect of loss of hyaluronan synthases on bone quality, suggesting an essential role hyaluronan plays during the development and regulation of bone.

1. Introduction

Hyaluronan is a nonsulfated glycosaminoglycan found in many tissues and is involved in regulating cellular processes, such as proliferation, and maintaining tissue structure. While the role of hyaluronan is relatively well-defined in some tissue types, like cartilage and skin, its role in bone is not as clear. For example, changes in hyaluronan are associated with bone diseases [1]; however, there is a lack of characterization of how endogenous hyaluronan production affects bone quality. Similarly, studies have identified roles for hyaluronan during development, specifically endochondral ossification [2–4], but there is little information on how it impacts bone morphology after growth. Others show that supplementation with exogenous hyaluronan inhibits osteoclastogenesis and bone resorption [5], while exogenous high molecular weight hyaluronan stimulates osteoblast activity, increasing cell mineralization [6]. Taken together, these studies highlight that, although hyaluronan plays a putative role in bone development and remodeling, it remains unclear how endogenous production of hyaluronan affects bone morphology and quality.

Hyaluronan is synthesized by three isoenzymes – hyaluronan synthases 1 (Has1), 2 (Has2), and 3 (Has3) – that produce hyaluronan of different molecular weight ranges [7]. The expression and activity of these synthases varies between tissue type and loss of any of these synthases affect growth and regeneration in skeletal and other tissues [8,9]. Loss of *Has2*, the major contributor for hyaluronan production during limb development [10], results in embryonic fatality [11]. *Has1*

* Corresponding author at: Weldon School of Biomedical Engineering, 206 S. Martin Jischke Drive, West Lafayette, IN 47907, United States of America.
E-mail address: chand@purdue.edu (D.D. Chan).
[1] Co-senior authors.

https://doi.org/10.1016/j.bone.2023.116779
Received 8 December 2022; Received in revised form 18 April 2023; Accepted 20 April 2023
Available online 24 April 2023

and *Has3* are necessary to regulate post-injury inflammation and cell behavior in the synovial joint [12] and skin [13]. *Has2* and *Has3* have been shown to be upregulated in tendons after injury [14] and loss of *Has1* has been shown to impact formation of the retrocalcaneal bursa [15]. All three synthases have been shown to be involved in endochondral ossification [16], suggesting that changes to hyaluronan synthesis would impact bone formation.

The three hyaluronan synthases have been shown to play some roles throughout bone growth, development and remodeling. Has2 and Has3 mediate hyaluronan synthesis from osteoblasts [17]. Human mineralizing osteoblast-like cells have decreased *HAS3* expression in vitro compared to non-mineralizing cells [17], suggesting that endogenous hyaluronan production by Has3 in mice could impact mineralization. A recent study has shown that a deficiency in hyaluronidase 1, an enzyme responsible for endogenous turnover of hyaluronan in the extracellular matrix, resulted in decreased bone mineral density (BMD), femoral length, and altered osteoblast and osteoclast activity [18]. Although these studies suggest that changes to endogenous hyaluronan production could lead to significant changes to bone quality and material properties, this association has not been directly studied. Therefore, the goal of this study is the characterize changes to bone morphology, matrix quality, and mechanics in mice deficient in *Has1* or *Has3*, noting that we cannot compare these to global knockout of Has2 due to embryonic fatality in those mice [11]. We hypothesized that alterations to endogenous hyaluronan production would deteriorate bone quality and strength by changing bone matrix composition.

2. Methods

2.1. Animals

Wildtype (WT, $n = 5$), *Has1*−/− ($n = 6$), [19] and *Has3*−/− ($n = 6$) [20] C57Bl/6 J female mice were bred and raised under an approved Institutional Animal Care and Use Committee protocol at Rensselaer Polytechnic Institute. *Has1*−/− and *Has3*−/− genetic lines were obtained as double-knockout C57Bl/6 J mice (generously gifted by Carol de la Motte) [21] and backcrossed to separate mutant alleles and achieve homozygous knockouts on the same genetic background. Genetic knockout was confirmed in breeders by genotyping for presence of mutant alleles for Has1 [19] and Has3 [20] and absence of wild-type alleles of the same. All mice were produced as homozygous offspring to homozygous parents. This study was limited to female mice due to unavailability of enough similarly aged males and cessation of our breeding colony during pandemic restrictions. Mice were housed with littermates on irradiated wood chip bedding, with standard enrichment (igloos) and provided ad libitum access to water and standard rodent chow (irradiated isoPro RMH 3000, LabDiet). Mice were euthanized at 12 weeks of age using CO_2 asphyxiation followed by confirmatory cervical dislocation. Both femora were collected, and all soft tissue was removed. Femora were then wrapped in saline-soaked gauze and stored in air-tight containers at −20 °C until testing.

2.2. Micro-computed tomography (microCT)

Femora were thawed and imaged with microCT (Scanco VivaCT 40, Switzerland) using imaging parameters of 70 kVp, 114 mA, 200-ms integration time, and 10.5-μM voxel size. A region of interest consisting of 30 cross-sectional slices (0.3-mm thick stack) was defined around the midshaft (beginning around 50 % of the length, extending 150 μm proximally and distally). BMD, cortical thickness, cortical bone area, marrow area, total bone area, bone area fraction, maximum moment of inertia (I_{max}), and minimum moment of inertia (I_{min}) were then calculated using a midshaft evaluation script that averages values across this volume of interest. Endosteal and periosteal diameters were measured using ImageJ at the midshaft slice.

2.3. Three-point bending

Left and right femora were loaded at a displacement-controlled loading rate of 0.05 mm/s under three-point bending until fracture (EnduraTec Elf 3200, TA Instruments, New Castle, DE). The span length (distance between the lower supports) was determined as half of the average bone length per group. The resulting load-displacement plot was used to calculate stiffness, maximum load, post-yield displacement, toughness, and work-to-fracture. Stiffness was identified as the slope of the linear region of the curve. The yield point was identified as the intersection of 10 % of the stiffness slope and the load-displacement plot. Ultimate (i.e., maximum) stress, yield stress, and elastic modulus was calculated from the load-displacement curve using standard engineering definitions [22]. The broken femora were stored at −20 °C for subsequent analyses.

2.4. Sample embedding

To prepare tissues for embedding, the proximal femoral epiphyses were cut using a low-speed circular saw (IsoMet 100, Buehler, Lake Bluff, IL). The marrow cavity was flushed using 1× phosphate-buffered saline (PBS) and were cleaned by submerging in a series of isopropyl ether, 70 % ethanol, and PBS for 15 min each. Samples were then dehydrated in 70 % ethanol overnight. After airdrying, the bones were placed in epoxy (Buehler Epothin 2) and were cured overnight. The epoxy molds were cut into 500 μm thick cross-sections using a low-speed circular saw. Sections were then polished across a gradient of carbide papers and diamond suspensions to a final surface finish of 1 μm.

2.5. Confocal Raman microscopy

Epoxy-embedded samples were imaged using a confocal Raman microscope (WiTec Alpha 300R, Oxford Instruments, Germany) with a green laser (532 nm) at high power (17 mW). Sixteen spectra were acquired for each sample (4 in each quadrant of the femur). The anterior, posterior, lateral, and medial quadrants were identified with a 20× objective, and spectra were obtained at 100× using the following parameters: grating at 600 g/mm, spectral center at 2100 cm^{-1}, 10 accumulations, and integration time of 1 s. Background fluorescence was removed with a polynomial fitting function and spectra were average for each sample in WiTec Project. Spectra were filtered using a 4th-order Savitsky-Golay filter at a window size of 9 in Matlab. The full-width at half-maximum (FWHM) intensities were measured for phosphate (v1PO43-, ~960 cm-1), carbonate (v1CO32-, ~1075 cm-1), amide I (~1600–1700 cm-1), and Amide III (~1240–1300 cm-1) peaks [23,24]. These values were used to calculate Amide *I* mineral-to-matrix ratio (phosphate/amide I), Amide III mineral-to-matrix ratio (phosphate/amide III), type B carbonate substitution (carbonate/phosphate), and crystallinity (1/phosphate). By capturing both amide peaks, we are able to assess mineral-to-matrix ratios regardless of polarization bias [25–27].

2.6. Nanoindentation

Following confocal Raman spectroscopy, nanoindentation was performed in the same embedded sections using a TI 900 Triboindenter (Bruker, Billerica, MA). The nanoindenter was calibrated following manufacturer's protocol to check transducer and stage performance using aluminum and quartz samples. Indents were performed using a Berkovich tip via the following load function: loading ramp at 300 μN/s, 6000 μN maximum load with a 30s hold, and unloading ramp at 300 μN/s [28]. Six indents in a line, spaced 10 μm apart, were performed across three regions on the samples [29] (Fig. S2A). The resulting unloading curve was analyzed using provided software (Bruker) using the Oliver-Pharr method, with the curve-fitting set to 95 % upper fit and 20 % lower fit for the unloading curve (Fig. S2B). Hardness and reduced

moduli measurements were averaged over these six repeated measures and three locations for each sample.

2.7. Quantification of fluorescent advanced glycation end-products (AGEs)

10 mg of cortical bone was cut from the distal end of femora after 3-point bending. Cut bones were then de-fatted and cleaned by agitating samples in 100 % isopropyl ether, 70 % ethanol, and saline for 15 min each. Samples were lyophilized and then hydrolyzed in 6 N HCl at 110 °C. The resulting hydrolysates were diluted 200× for quinine and hydroxyproline quantification. Flourescent AGEs were measured using a previously published protocol [23,30,31]. Triplicates of quinine sulphate standards and samples were dispensed in a black, flat-bottomed 96-well plate, and fluorescence was measured using a spectrophotometer (Biotek Synergy H4, Agilent, Santa Clara, CA) at 360 nm excitation and 460 nm emission. Collagen content was measured using a colorimetric assay [32]. Triplicates of L-hydroxyproline standards and samples were dispensed in a clear, flat-bottomed 96-well plate and absorbance was measured at 570 nm. The fluorescence of each sample was normalized to the amount of collagen, reported as ng quinine/mg collagen.

2.8. Histology

Distal femora were fixed in 4 % paraformaldehyde for 48 h and stored in PBS prior to preparation for histology. Fixed samples were demineralized in 14 % EDTA for 2 weeks and embedded in paraffin for sectioning. 5-μm sections were taken at the midshaft, starting at the fracture location from 3-point bending, and adjacent sections were stained with toluidine blue. Sections were imaged (Nikon TI Eclipse, Japan) and acquired (AmScope MU900, Irvine, CA) for analysis. Toluidine blue images were assessed for remodeling zones (reported as a ratio to cortical thickness) and bone-lining cells (reported as a ratio to total number of cells), following previously published protocols [33,34].

2.9. Statistical analysis

Data acquisition during above procedures was performed blinded to reduce bias. Statistical testing was performed in R [35] in RStudio [36], using $\alpha = 0.05$. MicroCT, three-point bending, and confocal Raman measurements for each mouse were averaged before running statistical analyses. AGE quantification was performed on one femur for each mouse. Normality was evaluated using a Shapiro-Wilk test, and variance was tested using a Bartlett or Levene test for normal or non-normal data, respectively. The effect of genotype on outcomes was tested using an ANOVA (normal datasets with equal variance), Welch ANOVA (normal datasets with unequal variance) or Kruskal-Wallis (non-normal datasets) test. Significant effects were tested for pairwise differences among groups using a Tukey's honest significant post-hoc for normal datasets or Dunn's test for non-normal datasets. Post-hoc power analysis was performed on G*Power [37,38] to determine effect size and power given the mean and variance for each metric (Table S1). Graphs were generated on GraphPad version 9.3.1 on MacOS.

Multivariate analysis was performed using R (mixOmics package [39]). Principal component analysis (PCA) was used to condense the dataset and to visualize metrics that influenced variance within groups. Partial least squares (PLS) regression models were used to predict mechanical behaviors from cortical bone morphometry and matrix composition and cortical bone morphometry from matrix composition. PLS regression models reduce the dimensionality of data to evaluate linear relationships between components. Initial PCAs were performed to determine the number of components that captured the variability of the dataset. The number of components was further tuned through a repeated cross-validated procedure.

3. Results

3.1. Cortical bone morphology

Loss of either *Has1* or *Has3* impacted some metrics of cortical bone morphology (Fig. 1, Table 1, Table S1); however, toluidine blue staining of histological sections did not reveal differences in bone cell counts, morphology, or apparent activity nor bone organization (Fig. S6). *Has1*$^{-/-}$ femora had significantly lower total bone area than WT (−9.54 %, $p = 0.0002$, Fig. 1E). *Has1*$^{-/-}$ bones had a significantly reduced marrow area compared to WT (−12.97 %, $p < 0.0001$, Fig. 1C). No significant genotype effects were found in cortical thickness, bone area (Fig. 1A,D), bone length, nor minimum moment of inertia (Table 1). Both *Has1*$^{-/-}$ and *Has3*$^{-/-}$ bones had a smaller endosteal diameters than WT (−11.27 %, p = 0.0002, and − 5.04 %, $p = 0.006$, respectively). Similar trends were seen in periosteal diameter (Table 1). Both *Has1*$^{-/-}$ (−21.49 %, $p = 0.0008$) and *Has3*$^{-/-}$ (−14.75 %, $p = 0.013$) bones had a lower maximum moment of inertia than WT bones (Table 1).

PCA of cortical bone morphometry revealed that PC1 and PC2 explained 99 % of the variability within the data (Fig. S4A). Clusters between *Has1*$^{-/-}$ and WT separated along PC2, which was mostly influenced by total bone area, endosteal and periosteal diameters. Has3$^{-/-}$ and WT were not separated along either axis.

3.2. Matrix content

Bone matrix content was evaluated using microCT and confocal Raman analysis (Fig. 2, Table S1). MicroCT revealed that BMD was significantly lower in Has3$^{-/-}$ bones compared to WT (−9.30 %, $p < 0.0001$) and *Has1*$^{-/-}$ (−7.41 %, p < 0.0001, Fig. 2A. Confocal Raman analysis showed that *Has1*$^{-/-}$ bones had a significantly lower amide I mineral-to-matrix ratio compared to WT bones (−15.30 %, p < 0.0001, Fig. 2B), while Has3$^{-/-}$ bones had a higher amide I mineral-to-matrix ratio than WT (+11.00 %, p < 0.0001). *Has1*$^{-/-}$ bones had a significantly lower amide III mineral-to-matrix ratio than WT bones (−82.24 %, p < 0.0001, Fig. 2C). *Has3*$^{-/-}$ bones had a significantly lower amount of type B carbonate substitution that WT bones (−19.51 %, $p = 0.002$, Fig. 2D). There were no significant differences in crystallinity between groups. Bulk fluorescent AGE content was significantly lower in *Has3*$^{-/-}$ bones than WT bones (−57.61 %, $p = 0.0478$), and unchanged in *Has1*$^{-/-}$ bones (Fig. 2F).

PCA showed that two components explained 99 % of the variance within matrix components; however, clusters between genotype were not well separated (Fig. S4B). PC1 was mostly influenced by AGE concentration, while PC2 was influenced by BMD.

3.3. Mechanical properties

Tissue-scale mechanical behavior was affected by loss of *Has3*, while loss of *Has1* had a more pronounced effect at the micron scale (Fig. 3, Table S1). *Has3*$^{-/-}$ bones had higher Young's modulus (+141.06 %, $p < 0.0001$, Fig. 3A) and stiffness (+61.34 %, p < 0.0001, Fig. 3B) but lower ultimate stress than WT bones (−41.30 %, $p = 0.0014$). Additionally, Has3−/− bones had a higher yield stress than WT bones ($p = 0.0373$). There were no significant differences in post-yield displacement nor work-to-fracture, and toughness among genotypes (Fig. S3). Reduced modulus was unchanged between groups (Fig. 3E), while *Has1*$^{-/-}$ bones showed significantly lower hardness when compared to WT bones (−45.42 %, $p = 0.033$, Fig. 3F).

PCA was dominated by PC1 and PC2, which explained over 99 % of the variance within the dataset. The Has3$^{-/-}$ cluster was separated from the WT cluster across PC1 and PC2 (Fig. S4C). PC1 was primarily influenced by ultimate stress, while PC2 was largely influenced by stiffness.

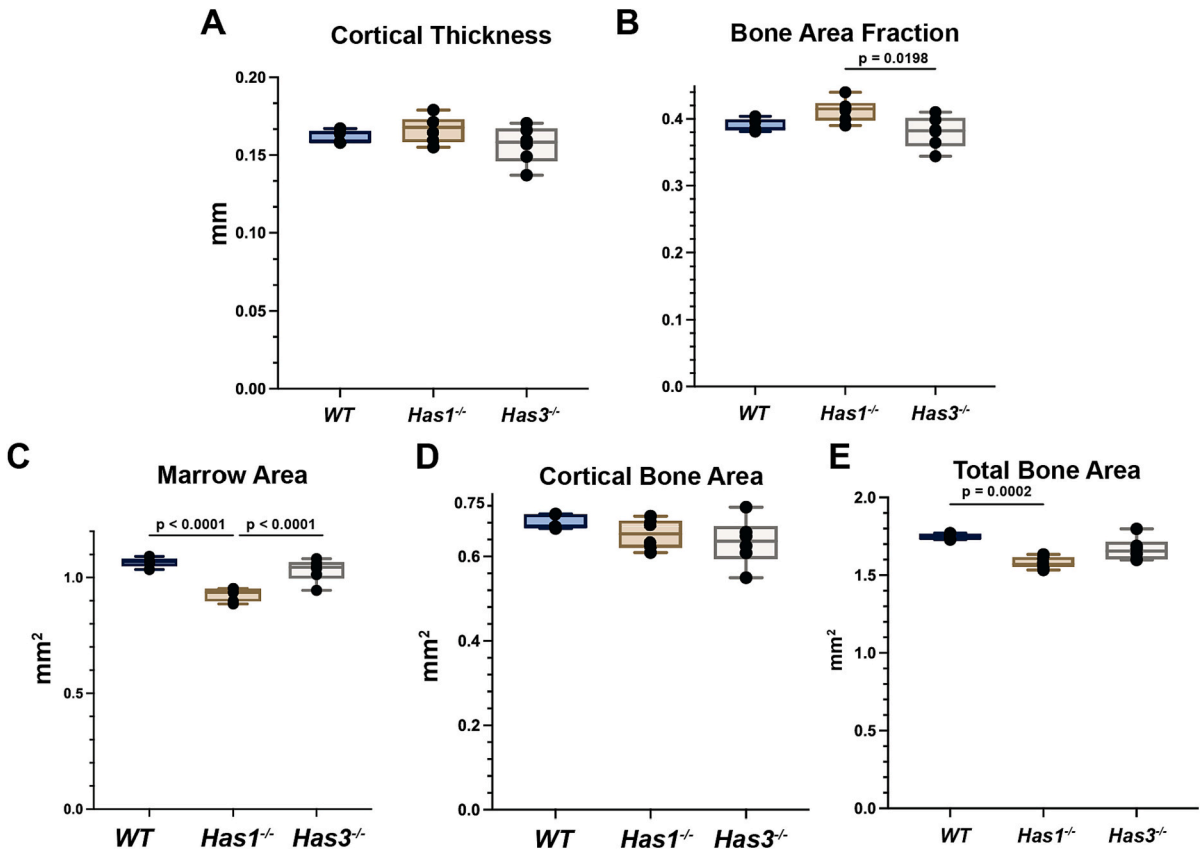

Fig. 1. Loss of either *Has1* or *Has3* alters cortical morphology. A) Cortical thickness was unaffected by genotype, while *Has1*−/− bones had significantly B) higher bone area fraction and C) lower marrow area compared to WT. D) Cortical bone area was similar among groups and E) total bone area was significantly lower in *Has1*$^{-/-}$ bones. Results are shown as boxplots, with median and interquartile range. Black circles represent average values from left and right femora for each mouse, with significant differences shown in brackets.

Table 1
Loss of Has1 or Has3 changes endosteal and periosteal expansion metrics. Has1−/− and Has3−/− bones have significantly lower maximum moments of inertia compared to WT bones while minimum moments of inertia were unchanged. Loss of both Has1 and Has3 resulted in significantly lower endosteal and periosteal diameters. Significant differences between groups ($p < 0.05$) are shown in sequential superscripts.

Genotype	Maximum moment of inertia (mm^4)	Minimum moment of inertia (mm^4)	Endosteal diameter (mm)	Periosteal diameter (mm)
WT	0.204 ± 0.010^{ab}	0.105 ± 0.001	1.411 ± 0.045^{cd}	1.800 ± 0.012^{ef}
Has1$^{-/-}$	0.160 ± 0.010^{a}	0.160 ± 0.007	1.252 ± 0.023^{c}	1.656 ± 0.023^{e}
Has3$^{-/-}$	0.174 ± 0.022^{b}	0.093 ± 0.010	1.340 ± 0.041^{d}	1.751 ± 0.043^{f}

3.4. Multivariate analysis

We used PLS regression models to evaluate how genetic perturbation may have changed how cortical bone morphometry and matrix composition influences bone mechanics. We trained three models: predicting cortical bone morphology from matrix composition (Fig. 4), predicting mechanical behavior from cortical bone traits (Fig. 5), and predicting mechanical properties from matrix components (Fig. 6).

When mapping matrix components on cortical bone morphometry, *Has3*$^{-/-}$ was distinctly separated from WT bones across component 2 (Fig. 4A, Fig. S5A). Component 2 was most influenced by BMD, cortical area, and cortical bone area fraction (Fig. 4D). When looking at the corresponding Pearson's correlation from features in the PLS model, BMD was positively correlated with cortical area, cortical bone area fraction, and cortical thickness (Fig. 4B).

In the model predicting mechanical properties from cortical bone morphometry, WT and *Has1*$^{-/-}$ bones were separated along component 1 (Fig. 5A, Fig. S5B). Component 1 was most heavily influenced by periosteal and endosteal diameters and micron-level mechanical properties (Fig. 5C). Periosteal and endosteal diameters were positively correlated with hardness and reduced modulus (Fig. 5B).

When projecting matrix components onto mechanical properties, clusters between WT and *Has3*$^{-/-}$ were separated along component 1 (Fig. 6A, Fig. S5C). Component 1 was influenced by BMD and ultimate stress (Fig. 6C), which were positively correlated (Fig. 6B).

4. Discussion

In this study, we showed that loss of hyaluronan synthases leads to multi-scale changes to bone morphology, matrix, and mechanics. We also demonstrated that loss of *Has1* impacts bone quality in a distinctly different manner from loss of *Has3*. Deficiency of *Has1* was associated with changes to cortical bone morphology and matrix content altering matrix-level hardness. *Has3*$^{-/-}$ bones showed a significant difference in matrix quality and morphology, leading to statistically significant differences compared to WT in whole-bone mechanical properties, but not micron-level mechanics. However, this does not exclude the possibility that there are other factors from the molecular to tissue scales that, although not measured in this study, may contribute to the macroscopic differences observed in whole-bone mechanical behaviors. Broadly, changes observed in bone structure, composition, and mechanics (Fig. 7) could be attributable to altered overall hyaluronan content or the loss of specific biological activity of either Has1 or Has3.

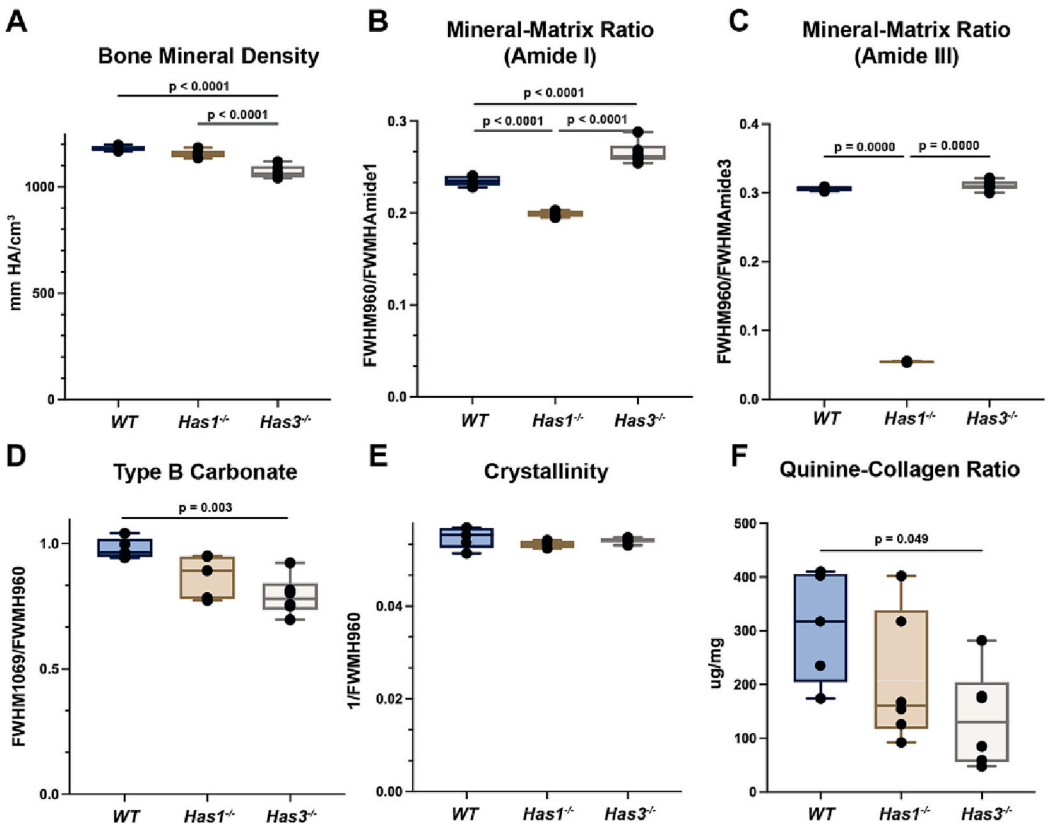

Fig. 2. Matrix composition varies with deficiency in *Has1* or *Has3*. A) Measurements from microCT revealed that loss of *Has1* or *Has3* significantly reduced bone mineral density compared to WT bones. Raman spectra were measured as full-width half-maximum (FWHM) ratios for peaks corresponding to the v1 phosphate at 960 nm, around the amide 1 (1616–1720 cm^{-1}) and amide 3 (1215–1300 cm^{-1}) peaks, and carbonate peak at 1069 nm. B) *Has1*−/− bones had a lower Amide I mineral-to-matrix ratio while *Has3*−/− bones had a higher Amide I mineral-to-matrix ratio compared to WT bones. C) *Has1*−/− bones had a significantly lower Amide III mineral-to-matrix compared to WT bones. D) *Has3* deficiency resulted in a significantly lower Type B Carbonate. E) Crystallinity was similar among groups. F) Quantification of fluorescent AGEs against quinine and hydroxyproline standards revealed that *Has3*−/− bones had the lowest AGE concentration. Results are shown as boxplots, with median and interquartile range. Black circles represent average values from left and right femora from each mouse, with significant differences shown in brackets.

4.1. Cortical bone morphology

There were striking differences in cortical morphology among WT, *Has1*$^{-/-}$, and *Has3*$^{-/-}$ bones. While longitudinal bone growth was not affected by genotype, marrow expansion may have been inhibited by loss of *Has1*, and accumulation of bone mass may have been affected by loss of *Has3*. Has1 deficient bones had significantly lower total bone area and marrow area, along with smaller periosteal and endosteal diameters compared to WT, suggesting periosteal expansion was suppressed during bone growth. Loss of *Has3* decreased bone area fraction along with endosteal and periosteal diameters relative to WT mice, which may be linked to the decrease in BMD. Downregulation of *HAS3* and reduction in hyaluronan production has been shown in human mineralizing osteoblasts [17]. This is also supported by the lower BMD in *Has3*$^{-/-}$ bones compared to both WT and *Has1*$^{-/-}$ bones.

Loss of bone in both *Has1*$^{-/-}$ and *Has3*$^{-/-}$ resulted a significantly lower maximum moment of inertia, which is close to the moment of inertia along the anteroposterior direction, suggesting that periosteal expansion was primarily limited in anteroposterior width. While we did not probe the mechanism behind the differences in cortical morphology here, work by others is suggestive. Hyaluronan may have an anti-osteoclastogenic effect through TLR4 [5], so altered hyaluronan synthesis could affect bone turnover. Alternatively, others have suggested that hyaluronan may modulate osteoclast-mediated bone resorption [40], potentially through interactions with parathyroid hormone [41,42]. Furthermore, mice lacking CD44, which is known to be activated by hyaluronan to increase *Rankl* expression [43], exhibit thicker cortical shell and smaller marrow area than wildtype controls, similar to the results in *Has1*$^{-/-}$ mice presented here. This supports the idea that changes to hyaluronan content or bioactivity may affect bone growth, homeostasis, and remodeling; however, further study is necessary to evaluate specific mechanisms.

4.2. Cortical bone composition

The difference in cortical BMD in knockout mice could also be explained by changes to mineral and matrix components. Mineral-to-matrix ratios can give an insight into the amount of mineral and collagen within the matrix and is related to BMD [44]. Loss of *Has3* showed an increase the amide I mineral-to-matrix ratio, despite a significant decrease in BMD. This suggests that collagen content may be significantly different in *Has3*$^{-/-}$ bones, perhaps compensating for reduced BMD. Some studies indicate that changes to the organic matrix may influence changes bone structure [45,46]. An increase in amide I mineral-to-matrix ratio with a corresponding loss of BMD was shown in a disuse model of osteoporosis [47] and in human osteogenesis imperfecta (OI) [48,49], a collagen-related bone disorder that alters hyaluronan content [1]. These associations with bone diseases support that idea that loss of *Has3* may lead to reduced BMD due to significant changes within the organic matrix composition of bone. Conversely, *Has1*$^{-/-}$ bones had lower amide I and amide III mineral-to-matrix ratios. *Has1*$^{-/-}$ bones also had a significantly lower hardness, which may be a result of the reduced mineral-to-matrix ratio. Lower hardness, as measured by nanoindentation in this work, has been associated with the reduced mineralization observed with osteomalacia [50], a finding that may suggest a similar relationship between hardness and mineralization in our study.

4.3. Cortical bone mechanics

While Has1$^{-/-}$ bones exhibited significant changes to hardness with nanoindentation, only *Has3*$^{-/-}$ bones showed distinct changes in whole bone mechanics with a significantly higher stiffness and elastic modulus than WT or *Has1*$^{-/-}$ bones. Nonenzymatic glycation of glycosaminoglycans, along with collagen, in articular cartilage has also been shown to contribute to increased tissue stiffness [51,52]. However, we observed

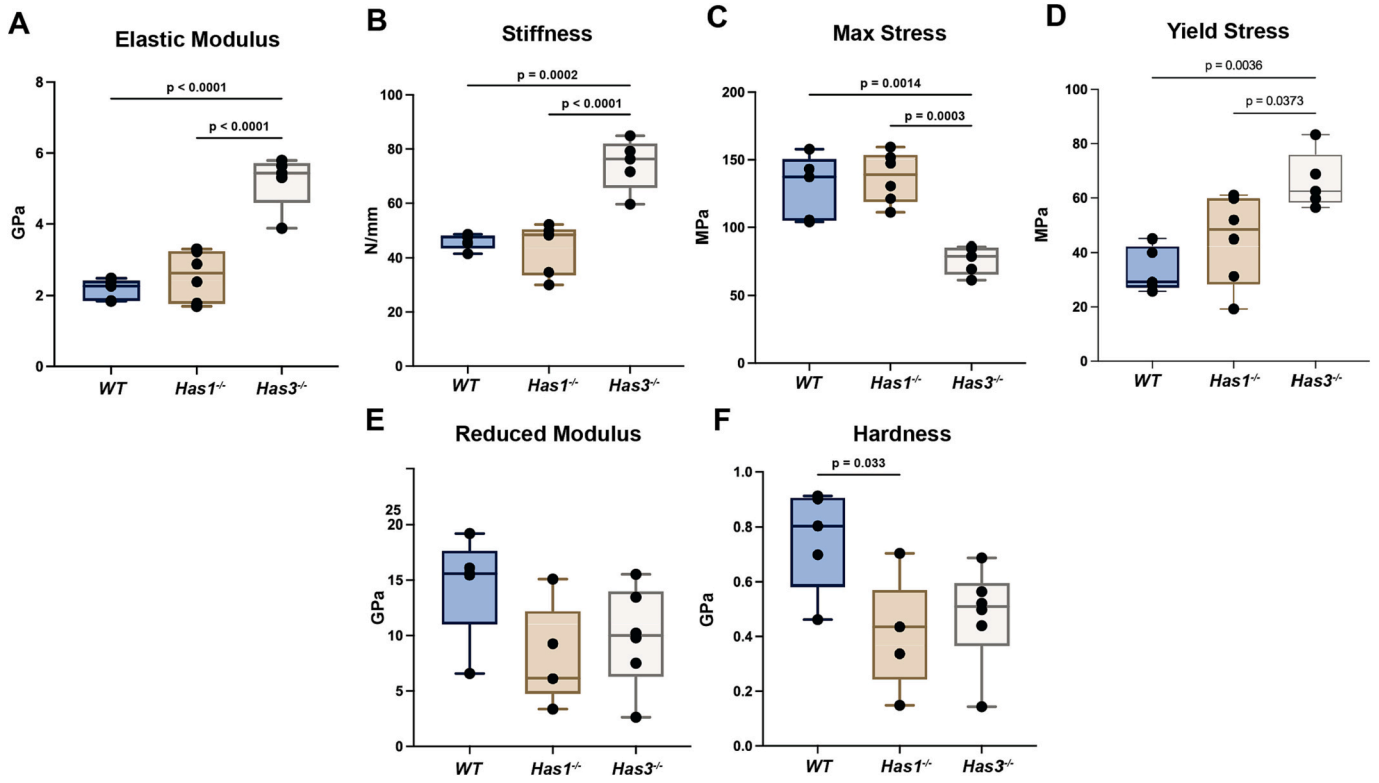

Fig. 3. Loss of *Has3* affects whole-tissue mechanical properties, while loss of *Has1* impacted micron-level hardness. Whole bone mechanical testing was done using three-point bending and the resulting load-displacement plot was used to assess mechanical behavior. Loss of *Has3* resulted in a significantly A) greater elastic modulus, B) greater stiffness, C) lower maximum stress, and D) greater yield stress. E) Nanoindentation revealed that loss of *Has1* or *Has3* did not affect reduced modulus. F) *Has1* deficiency resulted in significantly lower hardness. Results are shown as boxplots, with median and interquartile range. Black circles represent average values from left and right femurs for each mouse, with significant differences indicated with bars labeled with *p* values.

lower AGE content within *Has3*$^{-/-}$ bones, which were paradoxically stiffer than WT bones. One could speculate that the organic matrix composition, which includes the changes in AGE content, may be disrupting the normally direct relationship between BMD and modulus, perhaps via altered cortical porosity or mineral maturity, the latter supported by an observed decrease in carbonate. Our multivariate analysis showed that while AGE concentration was a predictor of ultimate stress, it was not a predictor of stiffness, suggesting that other matrix components had a larger impact on changes to mechanical properties. BMD was highly correlated with mechanics and the largest predictor of changes in mechanical behavior, implying instead that changes observed in *Has3*$^{-/-}$ were associated with altered mineralization.

Another potential explanation for altered mechanics is that there could be organizational differences in bone tissue due to altered hyaluronan content. Differences between lamellar and non-lamellar bone could result in different mechanical behavior under nanoindentation [53]. We noted no apparent differences in lamellar bone in histology, although our confocal Raman and nanoindenter imaging resolutions were not fine enough to resolve these differences at the exact locations of measurement. Although our histology results did not show appreciable differences in the calcified cartilage band within the bone of the different genotypes, mineralized regions of cartilage found in rodent long bones [54,55] could contribute to the differences in hardness measured by nanoindentation.

4.4. Altered bone phenotype interactions with loss of Has1

Phenotypic measurements of bone quality are inherently related, and we wanted to identify how changes in bone morphometry or matrix composition due to loss of *Has1* or *Has3* associated with altered mechanics (Fig. 7). Significant positive correlations were found among metrics associated with composition and both morphology and mechanics, as well as metrics of morphology associating with mechanics. The PLS regression model showed that *Has1*$^{-/-}$ bones could be distinguished from WT in their relationship between morphology and mechanics.

Changes in morphology due to the absence of *Has1* primarily influenced mechanical behaviors measured with nanoindentation, with periosteal and endosteal diameters positively correlated with hardness and reduced modulus. Rather than implying a directional relationship between morphology and material properties, this could suggest instead that the same underlying phenomenon that drives reduced hardness at the micron-scale also results in significantly smaller diameters of *Has1*$^{-/-}$ bones. Changes in osteocyte mechanobiology, resulting from reduced hyaluronan content in the matrix or absence of other Has1 activity, may be implicated because strong expression of CD44, a hyaluronan receptor, is found in osteocyte lacunae [56–58]. Prior work also suggests that hyaluronan-CD44 interactions may modulate osteocyte migration and cell-cell communication [59]. These interactions may also affect the transmission of mechanical cues from the extracellular matrix to osteocytes. Fibroblast transfection studies have demonstrated that CD44 is necessary to retain the hyaluronan-rich pericellular coat produced by HAS1 overexpression [60], although it remains unclear whether endogenous HAS1 activity and regulation, nor production of a pericellular coat, differ in bone cells. Taken together with evidence of a potential anti-osteoclastogenic effect of hyaluronan through TLR4 [5], these studies suggest that loss of Has1 in mice may alter bone cell behavior and mechanotransduction via changes to the pericellular coat and hyaluronan receptor interactions.

Furthermore, the Has1$^{-/-}$ genotype resulted in overall fewer interactions among the bone phenotypic measures evaluated in this study.

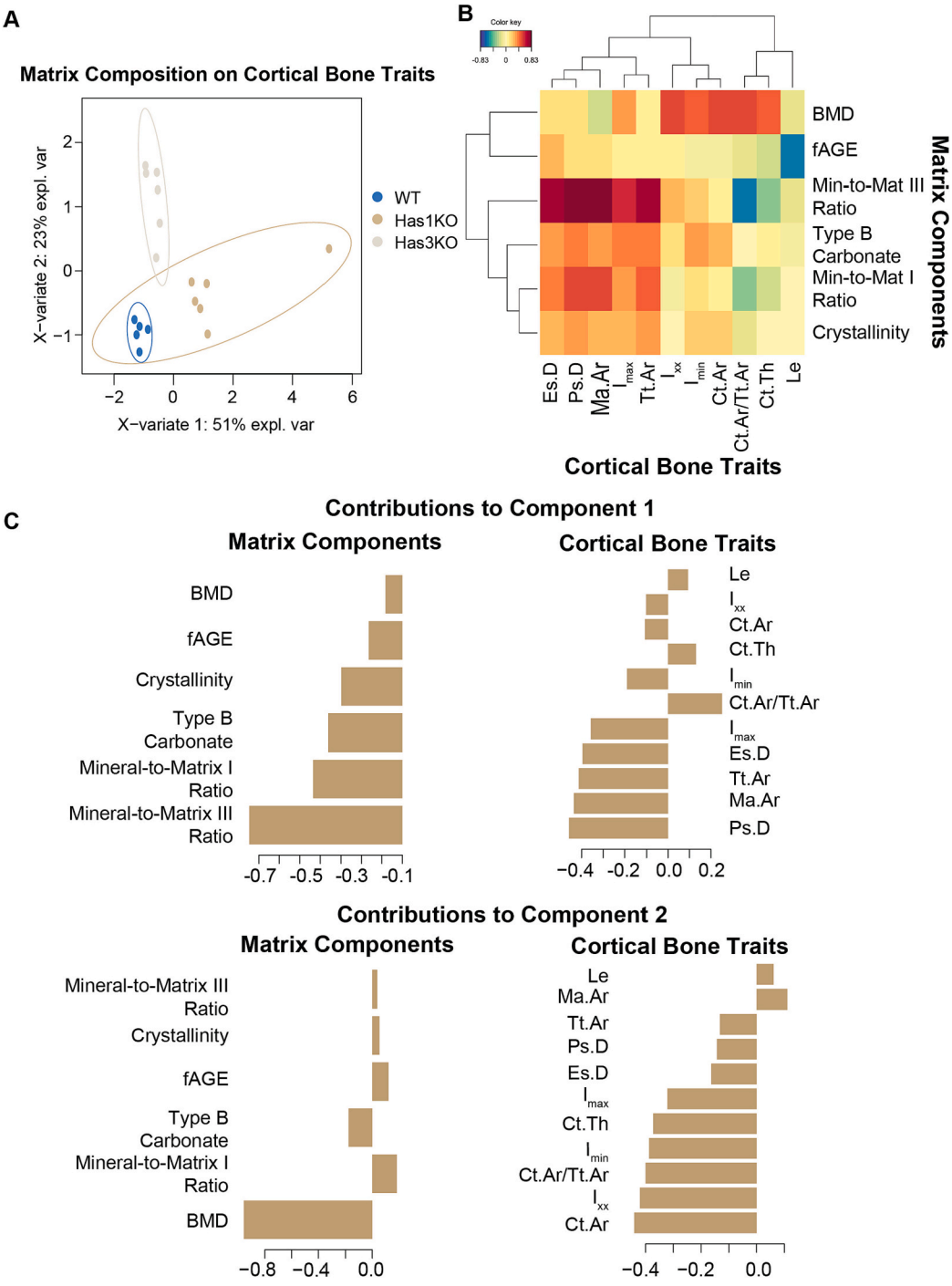

Fig. 4. Partial Least Squares (PLS) analysis of matrix components to predict cortical bone traits show distinct separation between *Has3*−/− bones and WT bones, where BMD influenced cortical area and thickness. A) PLS-Regression to predict cortical bone traits from matrix composition data, along with B) Pearson correlation coefficients between features in the two datasets derived from the PLS analysis. C) Corresponding loadings plots, showing the contributions of each metric for both components. PLS plots are shown in the X representative space of data along 2 components.

Has1 has been shown to require higher concentrations of glucosamine [61] or glucose [60] precursors or the presence of inflammatory signaling (i.e., IL-1β, TNFα, TGFβ) to produce a robust hyaluronan coat [60]. In addition, mesenchymal stem cells derived from human bone marrow express hyaluronan-rich pericellular coats but HAS1 showed the largest range of gene expression levels among the three isoenzymes [62], suggesting a higher sensitivity to systemic factors not measured in the human donors. These works imply that differences with the loss of Has1 may not manifest as strongly in normal or healthy bone but could be enhanced with high-sugar diet, inflammation, or injury [12], an intriguing association that remains to be studied in future work.

4.5. Altered bone phenotype interactions with loss of Has3

$Has3^{-/-}$ bones showed distinction from WT in both the composition to morphology and morphology to mechanics relationships (Fig. 7). Multivariate analysis with PLS regression models revealed that the changes in matrix composition due to *Has3* deficiency – particularly bone mineral content – influenced changes to cortical bone morphology and mechanics. While our PLS model predicting mechanical behaviors from cortical bone morphometry did not separate $Has3^{-/-}$ and WT bones, matrix components did associate to mechanical behaviors. This suggests that changes to matrix composition may have a greater influence on mechanical behaviors in *Has3* deficient bones than changes in cortical morphometry. Many studies, as reviewed previously [63], have

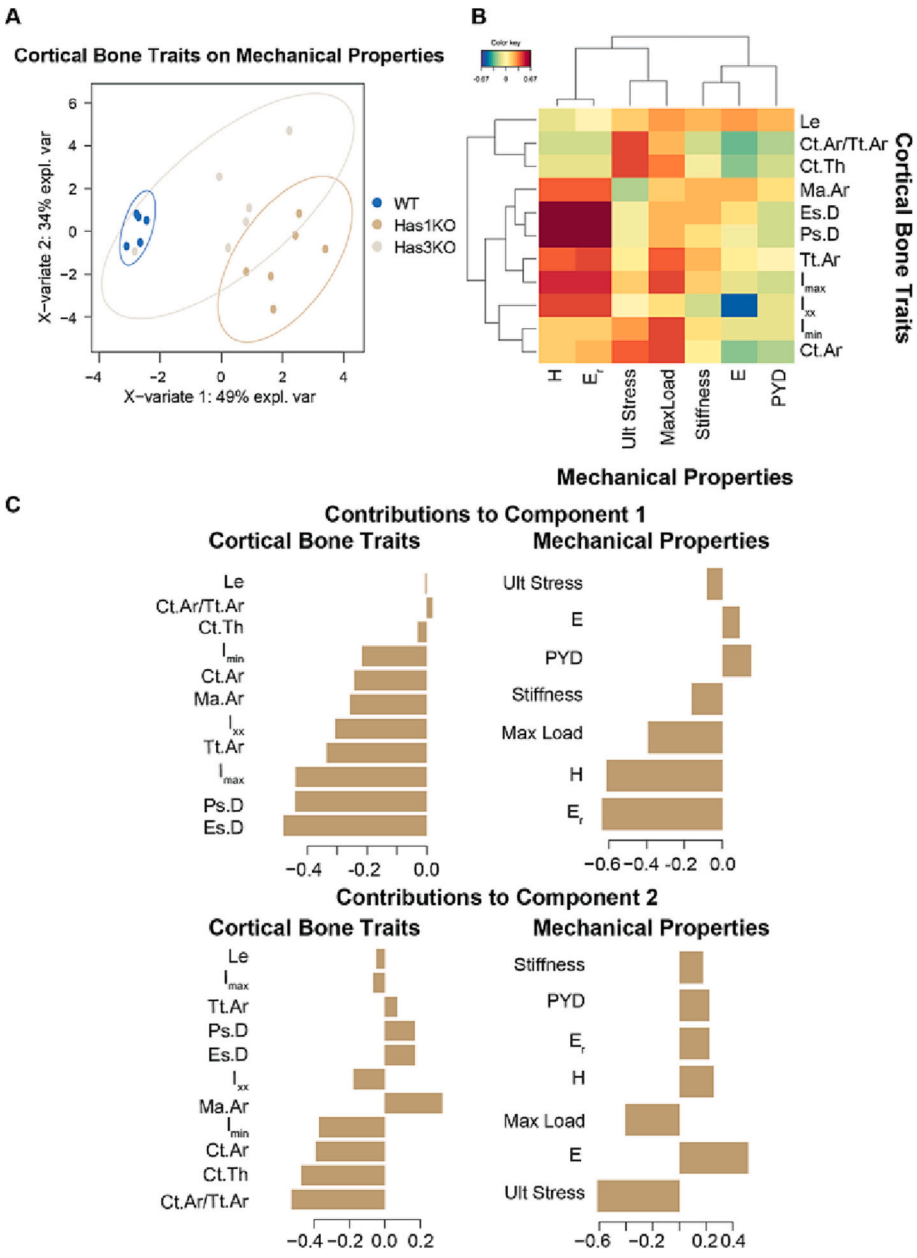

Fig. 5. Partial Least Squares (PLS) analysis of cortical bone traits to predict mechanical properties show distinct separation between *Has1*−/− bones and WT bones, where micron-level mechanical properties seem to be influenced by changes in endosteal and periosteal diameters. A) PLS-Regression to predict mechanical properties from cortical morphometric data, along with B) Pearson correlation coefficients between features in the two datasets derived from the PLS analysis. C) Corresponding loadings plots, showing the contributions of each metric for both components. PLS plots are shown in the X representative space of data along 2 components.

also shown strong correlations between matrix composition and mechanical behaviors, especially during aging, osteoporosis, and other pathologies.

BMD was correlated with cortical thickness and bone area measurements, and this relationship was a prominent differentiator of *Has3*$^{-/-}$ bones from WT bones. As with the significant associations observed in *Has1*$^{-/-}$ bones, the most likely explanation is that the same underlying phenomena affect both BMD and morphology in the *Has3*$^{-/-}$ bone. Beyond the downregulation of HAS3 observed in human mineralizing osteoblasts [17] already discussed above, studies in teeth also suggest a role for Has3 during the development of mineralized tissues. Has2 and Has3 express in spatially complementary patterns in tooth and craniofacial development in the embryonic mouse [64]. The role of Has3 in prenatal and postnatal hyaluronan synthesis in tooth development was also suggested to indicate a relationship to mineral transport into the enamel [65]. Separately, Has3 has also been strongly associated with hyaluronan coat formation [66] and regulation of bone-marrow derived hematopoietic [67] and mesenchymal [66] stem cells. Scanning electron microscopy and other approaches to examine organizational differences in bone may be used in future studies to probe a potential role for calcified cartilage islands [54,55], pericellular hyaluronan, and other potential explanations for a link between hyaluronan and mineralization.

4.6. Study limitations and future work

While knockout mouse models are a powerful tool to assess the function a gene plays within a tissue, it comes with the limitation that they only demonstrate the total effect of the loss of a gene. The exact function of *Has1* or *Has3* within development or growth will need to be further studied to understand the mechanisms behind the reported results. Because we used 12-week-old mice, this study is constrained to the cumulative effects of hyaluronan synthase expression during development and growth. This age is considered early adulthood and approximately equivalent to 20 years of age in humans [68]. Furthermore, while global knockouts provide strong evidence for a role of hyaluronan synthases and hyaluronan in the measured effects, bone cell type specific targeting of Has1, 2, or 3 could enable the evaluation of varying

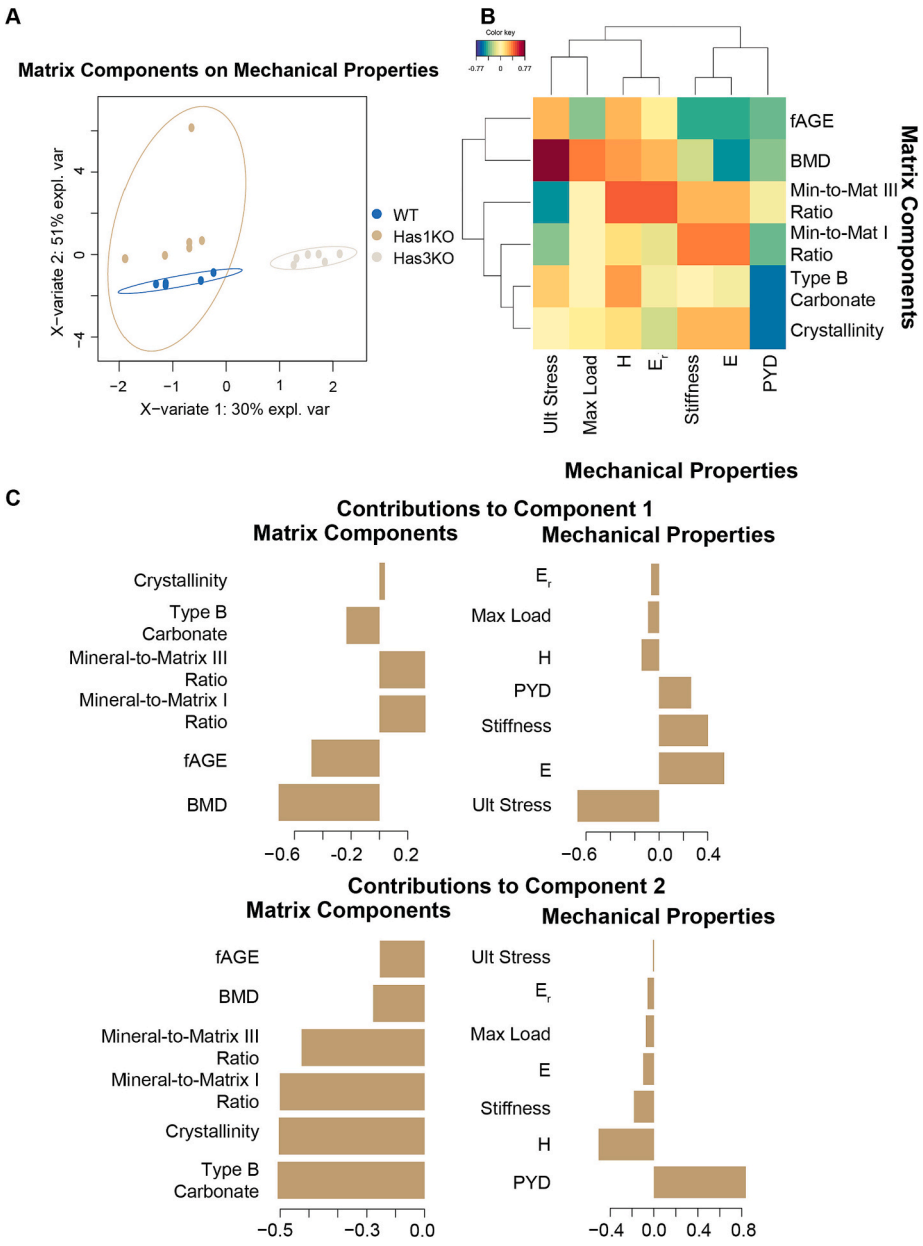

Fig. 6. Partial Least Squares (PLS) analysis of matrix components to predict mechanical properties show distinct separation between *Has3*−/− bones and WT bones, where changes in BMD influenced Max Stress. A) PLS-Regression to predict mechanical properties from matrix composition, along with B) Pearson correlation coefficients between features in the two datasets derived from the PLS analysis. C) Corresponding loadings plots, showing the contributions of each metric for both components. PLS plots are shown in the X representative space of data along 2 components.

hyaluronan synthase activities and hyaluronan signaling at the cellular level, as well as over the course of development and growth. In addition, although we found statistically significant differences among genotypes in mineral-matrix ratios, amide I and III peaks are highly sensitive to noise due to their inherently lower magnitudes compared to the v1 phosphate peak. Proximity of these peaks to the noise floor of the Raman spectrum can hinder peak quantification and therefore estimation of ratios of phosphate to amide I and III. Future work requires further optimization of confocal Raman spectroscopy parameters, via such as increased laser power, accumulations, and imaging time, to achieve higher signal-to-noise of the amide I and III peaks.

Altogether, these results and limitations of the current study motivate additional work to identify the structural and mechanical roles of hyaluronan within the bone, as well as its interactions with other bone matrix components. Continuing studies could incorporate dynamic histomorphometry, bone turnover markers, and gene expression, as well as interactions or crosstalk between bone and other tissue compartments of the joint, including hyaluronan-rich cartilage and synovial fluid. This study is also limited to female mice at a specific age, so future work could endeavor to untangle the hyaluronan-linked and sex- and age-related phenotypes in bone using these same genetic models or others, including Has2 conditional [69] or heterozygous knockouts [70]. Motivated by the results of this work, future studies to characterize matrix changes due to hyaluronan deficiency throughout development and aging may reveal more roles that hyaluronan plays in bone.

4.7. Conclusion

In summary, here we have shown that loss of *Has1* or *Has3* has distinct effects on bone matrix composition, morphology, and mechanics (Fig. 7). This is the first study to identify the effect of altered hyaluronan synthesis on bone quality, motivating further studies on the role of hyaluronan within bone development and remodeling. Absence of *Has1* impacted morphology, mineralization, and hardness, suggesting that *Has1* may have a role in periosteal and endosteal expansion and the degree of mineralization in the matrix. *Has3* knockout was associated with diminished bone mineral density and altered organic matrix composition, impacting whole bone mechanics, suggesting that *Has3* is

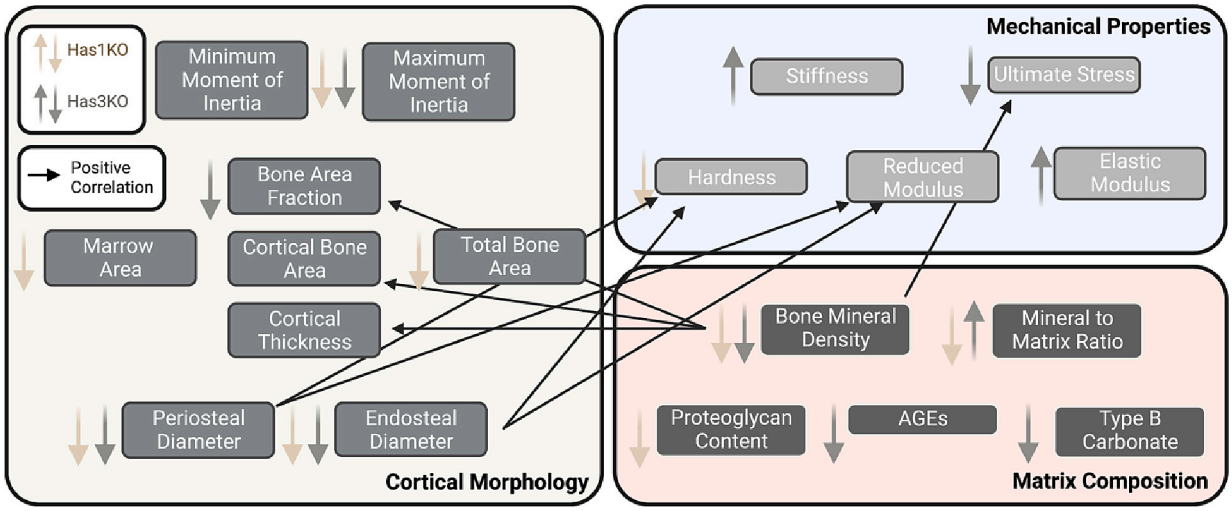

Fig. 7. Significant results for each genotype indicate potentially divergent mechanisms for hyaluronan synthase modulation of bone. Proposed relationship between cortical morphology, matrix composition, and mechanical properties based on significant features found through multivariate analysis. Light brown arrows indicate change in *Has1*$^{-/-}$ bones compared to WT, dark grey arrows indicate change in *Has3*$^{-/-}$ bones compared to WT. Black arrows indicate positive correlation between metrics found with PLS regression models. Created in Biorender. (For interpretation of the references to colour in this figure legend, the reader is referred to the web version of this article.)

necessary for bone matrix composition and structure. Our results show that endogenous production of hyaluronan is important for bone mineralization and matrix composition and motivate further studies to assess the role of hyaluronan during bone development and remodeling.

CRediT authorship contribution statement

Meghana Pendyala: Conceptualization, Data curation, Formal analysis, Investigation, Software, Visualization, Writing – original draft, Writing – review & editing. **Samuel J. Stephen:** Investigation, Data curation, Formal analysis, Investigation, Software, Writing – review & editing. **Deepak Vashishth:** Project administration, Supervision, Resources, Writing – review & editing. **Elizabeth A. Blaber:** Funding acquisition, Resources, Validation, Writing – review & editing. **Deva D. Chan:** Conceptualization, Funding acquisition, Project administration, Resources, Supervision, Writing – review & editing.

Declaration of competing interest

None.

Data availability

Data will be made available on request.

Acknowledgements

The authors acknowledge the following core facilities and personnel for their assistance to this study: Drs. Neda Bajalo and Antigone McKenna in the BioResearch Core, Dr. Scott McCallum in the Bio-Imaging Core, and Dr. Deniz Rende in the Polymer Processing Core at Rensselaer Polytechnic Institute. We also acknowledge Drs. Lilian Plotkin and Drew Brown of the Histology and the Bone and Body Composition Cores of the IU School of Medicine. We would also like to acknowledge Dr. Douglas Brubaker for assistance with multivariate analysis and Rukmani Cahill for assistance with experimental protocols.

Funding sources

This work was supported by National Science Foundation through Awards 1944394, 2149946, 0722563, and through an MRI Grant DMR-2019273001.

Appendix A. Supplementary data

Supplementary data to this article can be found online at https://doi.org/10.1016/j.bone.2023.116779.

References

[1] A. Oohira, H. Nogami, Elevated accumulation of hyaluronate in the tubular bones of osteogenesis imperfecta, Bone 10 (6) (1989) 409–413.
[2] P. Pavasant, T. Shizari, C.B. Underhill, Hyaluronan contributes to the enlargement of hypertrophic lacunae in the growth plate, J. Cell Sci. 109 (Pt 2) (1996) 327–334.
[3] M. Shimoda, H. Yoshida, S. Mizuno, T. Hirozane, K. Horiuchi, Y. Yoshino, H. Hara, Y. Kanai, S. Inoue, M. Ishijima, Y. Okada, Hyaluronan-binding protein involved in hyaluronan depolymerization controls endochondral ossification through hyaluronan metabolism, Am. J. Pathol. 187 (5) (2017) 1162–1176.
[4] P. Moffatt, E.R. Lee, B. St-Jacques, K. Matsumoto, Y. Yamaguchi, P.J. Roughley, Hyaluronan production by means of Has2 gene expression in chondrocytes is essential for long bone development, Dev. Dyn. 240 (2) (2011) 404–412.
[5] E.J. Chang, H.J. Kim, J. Ha, H.J. Kim, J. Ryu, K.H. Park, U.H. Kim, Z.H. Lee, H. M. Kim, D.E. Fisher, H.H. Kim, Hyaluronan inhibits osteoclast differentiation via toll-like receptor 4, J. Cell Sci. 120 (Pt 1) (2007) 166–176.
[6] L. Huang, Y.Y. Cheng, P.L. Koo, K.M. Lee, L. Qin, J.C. Cheng, S.M. Kumta, The effect of hyaluronan on osteoblast proliferation and differentiation in rat calvarial-derived cell cultures, J. Biomed. Mater. Res. A 66 (4) (2003) 880–884.
[7] N. Itano, K. Kimata, Mammalian hyaluronan synthases, IUBMB Life 54 (4) (2002) 195–199.
[8] N. Itano, T. Sawai, M. Yoshida, P. Lenas, Y. Yamada, M. Imagawa, T. Shinomura, M. Hamaguchi, Y. Yoshida, Y. Ohnuki, S. Miyauchi, A.P. Spicer, J.A. McDonald, K. Kimata, Three isoforms of mammalian hyaluronan synthases have distinct enzymatic properties, J. Biol. Chem. 274 (35) (1999) 25085–25092.
[9] H. Siiskonen, S. Oikari, S. Pasonen-Seppanen, K. Rilla, Hyaluronan synthase 1: a mysterious enzyme with unexpected functions, Front. Immunol. 6 (2015) 43.
[10] Y. Li, B.P. Toole, C.N. Dealy, R.A. Kosher, Hyaluronan in limb morphogenesis, Dev. Biol. 305 (2) (2007) 411–420.
[11] T.D. Camenisch, A.P. Spicer, T. Brehm-Gibson, J. Biesterfeldt, M.L. Augustine, A. Calabro Jr., S. Kubalak, S.E. Klewer, J.A. McDonald, Disruption of hyaluronan synthase-2 abrogates normal cardiac morphogenesis and hyaluronan-mediated transformation of epithelium to mesenchyme, J. Clin. Invest. 106 (3) (2000) 349–360.
[12] D.D. Chan, W.F. Xiao, J. Li, C.A. de la Motte, J.D. Sandy, A. Plaas, Deficiency of hyaluronan synthase 1 (Has1) results in chronic joint inflammation and widespread intra-articular fibrosis in a murine model of knee joint cartilage damage, Osteoarthr. Cartil. 23 (11) (2015) 1879–1889.
[13] J.A. Mack, R.J. Feldman, N. Itano, K. Kimata, M. Lauer, V.C. Hascall, E.V. Maytin, Enhanced inflammation and accelerated wound closure following tetraphorbol ester application or full-thickness wounding in mice lacking hyaluronan synthases Has1 and Has3, J. Invest. Dermatol. 132 (1) (2012) 198–207.

[14] M. Berglund, D.A. Hart, M. Wiig, The inflammatory response and hyaluronan synthases in the rabbit flexor tendon and tendon sheath following injury, J. Hand Surg. Eur. Vol. 32 (5) (2007) 581–587.
[15] K.J. Sikes, K. Renner, J. Li, K.J. Grande-Allen, J.P. Connell, V. Cali, R.J. Midura, J. D. Sandy, A. Plaas, V.M. Wang, Knockout of hyaluronan synthase 1, but not 3, impairs formation of the retrocalcaneal bursa, J. Orthop. Res. 36 (10) (2018) 2622–2632.
[16] Y. Takada, H. Sakiyama, K. Kuriiwa, R. Masuda, N. Inoue, K. Nakagawa, N. Itano, T. Saito, T. Yamada, K. Kimata, Metabolic activities of partially degenerated hypertrophic chondrocytes: gene expression of hyaluronan synthases, Cell Tissue Res. 298 (2) (1999) 317–325.
[17] J.R. Adams, G. Sander, S. Byers, Expression of hyaluronan synthases and hyaluronidases in the MG63 osteoblast cell line, Matrix Biol. 25 (1) (2006) 40–46.
[18] E. Puissant, F. Gilis, V. Tevel, J.M. Vandeweerd, B. Flamion, M. Jadot, M. Boonen, Hyaluronidase 1 deficiency decreases bone mineral density in mice, Sci. Rep. 12 (1) (2022) 10142.
[19] N. Kobayashi, S. Miyoshi, T. Mikami, H. Koyama, M. Kitazawa, M. Takeoka, K. Sano, J. Amano, Z. Isogai, S. Niida, K. Oguri, M. Okayama, J.A. McDonald, K. Kimata, S. Taniguchi, N. Itano, Hyaluronan deficiency in tumor stroma impairs macrophage trafficking and tumor neovascularization, Cancer Res. 70 (18) (2010) 7073–7083.
[20] K.J. Bai, A.P. Spicer, M.M. Mascarenhas, L. Yu, C.D. Ochoa, H.G. Garg, D.A. Quinn, The role of hyaluronan synthase 3 in ventilator-induced lung injury, Am. J. Respir. Crit. Care Med. 172 (1) (2005) 92–98.
[21] S.P. Kessler, D.R. Obery, C. de la Motte, Hyaluronan synthase 3 null mice exhibit decreased intestinal inflammation and tissue damage in the DSS-induced colitis model, Int. J. Cell Biol. 2015 (2015), 745237.
[22] K.J. Jepsen, M.J. Silva, D. Vashishth, X.E. Guo, M.C. van der Meulen, Establishing biomechanical mechanisms in mouse models: practical guidelines for systematically evaluating phenotypic changes in the diaphyses of long bones, J. Bone Miner. Res. 30 (6) (2015) 951–966.
[23] J.E. LLabre, G.E. Sroga, M.J.L. Tice, D. Vashishth, Induction and rescue of skeletal fragility in a high-fat diet mouse model of type 2 diabetes: an in vivo and in vitro approach, Bone 156 (2022), 116302.
[24] M.J.L. Tice, S. Bailey, G.E. Sroga, E.J. Gallagher, D. Vashishth, Non-obese MKR mouse model of type 2 diabetes reveals skeletal alterations in mineralization and material properties, JBMR Plus 6 (2) (2022), e10583.
[25] M. Kazanci, P. Roschger, E.P. Paschalis, K. Klaushofer, P. Fratzl, Bone osteonal tissues by raman spectral mapping: orientation-composition, J. Struct. Biol. 156 (3) (2006) 489–496.
[26] S. Schrof, P. Varga, L. Galvis, K. Raum, A. Masic, 3D raman mapping of the collagen fibril orientation in human osteonal lamellae, J. Struct. Biol. 187 (3) (2014) 266–275.
[27] A.J. Makowski, C.A. Patil, A. Mahadevan-Jansen, J.S. Nyman, Polarization control of raman spectroscopy optimizes the assessment of bone tissue, J. Biomed. Opt. 18 (5) (2013) 55005.
[28] M. Casanova, A. Balmelli, D. Carnelli, D. Courty, P. Schneider, R. Muller, Nanoindentation analysis of the micromechanical anisotropy in mouse cortical bone, R. Soc. Open Sci. 4 (2) (2017), 160971.
[29] R. Lucchini, D. Carnelli, M. Ponzoni, E. Bertarelli, D. Gastaldi, P. Vena, Role of damage mechanics in nanoindentation of lamellar bone at multiple sizes: experiments and numerical modeling, J. Mech. Behav. Biomed. Mater. 4 (8) (2011) 1852–1863.
[30] D. Vashishth, Advanced glycation end-products and bone fractures, IBMS Bonekey 6 (8) (2009) 268–278.
[31] D. Vashishth, G.J. Gibson, J.I. Khoury, M.B. Schaffler, J. Kimura, D.P. Fyhrie, Influence of nonenzymatic glycation on biomechanical properties of cortical bone, Bone 28 (2) (2001) 195–201.
[32] G.E. Sroga, D. Vashishth, UPLC methodology for identification and quantitation of naturally fluorescent crosslinks in proteins: a study of bone collagen, J. Chromatogr. B Anal. Technol. Biomed. Life Sci. 879 (5–6) (2011) 379–385.
[33] R.G. Erben, M. Glosmann, Histomorphometry in rodents, Methods Mol. Biol. 816 (2012) 279–303.
[34] M. Askmyr, N.A. Sims, T.J. Martin, L.E. Purton, What is the true nature of the osteoblastic hematopoietic stem cell niche? Trends Endocrinol. Metab. 20 (6) (2009) 303–309.
[35] R Development Core Team, R: A Language and Environment for Statistical Computing, R Foundation for Statistical Computing, Vienna, Austra, 2010.
[36] RStudio Team, RStudio: Integrated Development for R, RStudio, PBC, Boston, MA, 2020.
[37] F. Faul, E. Erdfelder, A.G. Lang, A. Buchner, G*Power 3: a flexible statistical power analysis program for the social, behavioral, and biomedical sciences, Behav. Res. Methods 39 (2) (2007) 175–191.
[38] H. Kang, Sample size determination and power analysis using the G*Power software, J. Educ. Eval. Health Prof. 18 (2021) 17.
[39] F. Rohart, B. Gautier, A. Singh, K.A. Le Cao, mixOmics: an R package for 'omics feature selection and multiple data integration, PLoS Comput. Biol. 13 (11) (2017), e1005752.
[40] C.W. Prince, Roles of hyaluronan in bone resorption, BMC Musculoskelet. Disord. 5 (2004) 12.
[41] R.A. Luben, J.F. Goggins, L.G. Raisz, Stimulation by parathyroid hormone of bone hyaluronate synthesis in organ culture, Endocrinology 94 (3) (1974) 737–745.
[42] J.A. Wener, S.J. Gorton, L.G. Raisz, Escape from inhibition or resorption in cultures of fetal bone treated with calcitoninand parathyroid hromone, Endocrinology 90 (3) (1972) 752–759.
[43] J.J. Cao, P.A. Singleton, S. Majumdar, B. Boudignon, A. Burghardt, P. Kurimoto, T. J. Wronski, L.Y. Bourguignon, B.P. Halloran, Hyaluronan increases RANKL expression in bone marrow stromal cells through CD44, J. Bone Miner. Res. 20 (1) (2005) 30–40.
[44] M. Unal, Raman spectroscopic determination of bone matrix quantity and quality augments prediction of human cortical bone mechanical properties, J. Biomech. 119 (2021), 110342.
[45] X.X. Wen, F.Q. Wang, C. Xu, Z.X. Wu, Y. Zhang, Y.F. Feng, Y.B. Yan, W. Lei, Time related changes of mineral and collagen and their roles in cortical bone mechanics of ovariectomized rabbits, PLoS One 10 (6) (2015), e0127973.
[46] S. Rokidi, E.P. Paschalis, K. Klaushofer, S. Vennin, A. Desyatova, J.A. Turner, P. Watson, J. Lappe, M.P. Akhter, R.R. Recker, Organic matrix quality discriminates between age- and BMD-matched fracturing versus non-fracturing post-menopausal women: a pilot study, Bone 127 (2019) 207–214.
[47] Y. Ishimaru, Y. Oshima, Y. Imai, T. Iimura, S. Takanezawa, K. Hino, H. Miura, Raman spectroscopic analysis to detect reduced bone quality after sciatic neurectomy in mice, Molecules 23 (12) (2018).
[48] L. Imbert, J.C. Auregan, K. Pernelle, T. Hoc, Mechanical and mineral properties of osteogenesis imperfecta human bones at the tissue level, Bone 65 (2014) 18–24.
[49] S. Tournis, A.D. Dede, Osteogenesis imperfecta - a clinical update, Metabolism 80 (2018) 27–37.
[50] I. Hadjab, D. Farlay, P. Crozier, T. Douillard, G. Boivin, J. Chevalier, S. Meille, H. Follet, Intrinsic properties of osteomalacia bone evaluated by nanoindentation and FTIRM analysis, J. Biomech. 117 (2021), 110247.
[51] P.R. Moshtagh, N.M. Korthagen, M.H.P. van Rijen, R.M. Castelein, A.A. Zadpoor, H. Weinans, Effects of non-enzymatic glycation on the micro- and nano-mechanics of articular cartilage, J. Mech. Behav. Biomed. Mater. 77 (2018) 551–556.
[52] N. Verzijl, J. DeGroot, Z.C. Ben, O. Brau-Benjamin, A. Maroudas, R.A. Bank, J. Mizrahi, C.G. Schalkwijk, S.R. Thorpe, J.W. Baynes, J.W. Bijlsma, F.P. Lafeber, J. M. TeKoppele, Crosslinking by advanced glycation end products increases the stiffness of the collagen network in human articular cartilage: a possible mechanism through which age is a risk factor for osteoarthritis, Arthritis Rheum. 46 (1) (2002) 114–123.
[53] V.D. Sherk, C.M. Heveran, R.M. Foright, G.C. Johnson, D.M. Presby, V.L. Ferguson, P.S. MacLean, Sex differences in the effect of diet, obesity, and exercise on bone quality and fracture toughness, Bone 145 (2021), 115840.
[54] F.L. Bach-Gansmo, S.C. Irvine, A. Bruel, J.S. Thomsen, H. Birkedal, Calcified cartilage islands in rat cortical bone, Calcif. Tissue Int. 92 (4) (2013) 330–338.
[55] V. Ip, Z. Toth, J. Chibnall, S. McBride-Gagyi, Remnant woven bone and calcified cartilage in mouse bone: differences between Ages/Sex and effects on bone strength, PLoS One 11 (11) (2016), e0166476.
[56] D.E. Hughes, D.M. Salter, R. Simpson, CD44 expression in human bone: a novel marker of osteocytic differentiation, J. Bone Miner. Res. 9 (1) (1994) 39–44.
[57] H. Nakamura, S. Kenmotsu, H. Sakai, H. Ozawa, Localization of CD44, the hyaluronate receptor, on the plasma membrane of osteocytes and osteoclasts in rat tibiae, Cell Tissue Res. 280 (2) (1995) 225–233.
[58] K.J. Noonan, J.W. Stevens, R. Tammi, M. Tammi, J.A. Hernandez, R.J. Midura, Spatial distribution of CD44 and hyaluronan in the proximal tibia of the growing rat, J. Orthop. Res. 14 (4) (1996) 573–581.
[59] P. Spessotto, F.M. Rossi, M. Degan, R. Di Francia, R. Perris, A. Colombatti, V. Gattei, Hyaluronan-CD44 interaction hampers migration of osteoclast-like cells by down-regulating MMP-9, J. Cell Biol. 158 (6) (2002) 1133–1144.
[60] H. Siiskonen, R. Karna, J.M. Hyttinen, R.H. Tammi, M.I. Tammi, K. Rilla, Hyaluronan synthase 1 (HAS1) produces a cytokine-and glucose-inducible, CD44-dependent cell surface coat, Exp. Cell Res. 320 (1) (2014) 153–163.
[61] K. Rilla, S. Oikari, T.A. Jokela, J.M. Hyttinen, R. Karna, R.H. Tammi, M.I. Tammi, Hyaluronan synthase 1 (HAS1) requires higher cellular UDP-GlcNAc concentration than HAS2 and HAS3, J. Biol. Chem. 288 (8) (2013) 5973–5983.
[62] C. Qu, K. Rilla, R. Tammi, M. Tammi, H. Kroger, M.J. Lammi, Extensive CD44-dependent hyaluronan coats on human bone marrow-derived mesenchymal stem cells produced by hyaluronan synthases HAS1, HAS2 and HAS3, Int. J. Biochem. Cell Biol. 48 (2014) 45–54.
[63] M. Unal, A. Creecy, J.S. Nyman, The role of matrix composition in the mechanical behavior of bone, Curr. Osteoporos. Rep. 16 (3) (2018) 205–215.
[64] J.Y. Tien, A.P. Spicer, Three vertebrate hyaluronan synthases are expressed during mouse development in distinct spatial and temporal patterns, Dev. Dyn. 233 (1) (2005) 130–141.
[65] T. Morita, K. Fujikawa, O. Baba, S. Shibata, An in situ hybridization study of hyaluronan synthase (Has) mRNA in developing mouse molar and incisor tooth germs, Gene Expr. Patterns 21 (1) (2016) 28–40.
[66] S. Reiprich, E. Hofbauer, S. Kiderlen, H. Clausen-Schaumann, W. Bocker, A. Aszodi, V. Schonitzer, Adhesive properties of the hyaluronan pericellular coat in hyaluronan synthases overexpressing mesenchymal stem cells, Int. J. Mol. Sci. 21 (11) (2020).
[67] D.N. Haylock, S.K. Nilsson, The role of hyaluronic acid in hemopoietic stem cell biology, Regen. Med. 1 (4) (2006) 437–445.
[68] K. Flurkey, J.M. Currer, D.E. Harrison, Chapter 20 - mouse models in aging research, in: J.G. Fox, M.T. Davisson, F.W. Quimby, S.W. Barthold, C.E. Newcomer,

A.L. Smith (Eds.), The Mouse in Biomedical Research, Second Edition, Academic Press, Burlington, 2007, pp. 637–672.
[69] K. Matsumoto, Y. Li, C. Jakuba, Y. Sugiyama, T. Sayo, M. Okuno, C.N. Dealy, B. P. Toole, J. Takeda, Y. Yamaguchi, R.A. Kosher, Conditional inactivation of Has2 reveals a crucial role for hyaluronan in skeletal growth, patterning, chondrocyte maturation and joint formation in the developing limb, Development 136 (16) (2009) 2825–2835.
[70] M.T. Sherpa, T. Kiwamoto, M. Matsuyama, Y. Tsunoda, K. Yazaki, K. Yoshida, M. Nakajima, Y. Matsuno, Y. Morishima, Y. Ishii, N. Hizawa, Has2 regulates the development of ovalbumin-induced airway remodeling and steroid insensitivity in mice, Front. Immunol. 12 (2021), 770305.